

1 **Playing with FiRE: A genome resolved view of the soil microbiome responses to high** 2 **severity forest wildfire**

3 Amelia R. Nelson¹, Adrienne B. Narrowe¹, Charles C. Rhoades², Timothy S. Fegel², Rebecca A.
4 Daly¹, Holly K. Roth³, Rosalie K. Chu⁴, Kaela K. Amundson¹, Sara E. Geonczy⁵, Joanne B.
5 Emerson⁵, Robert B. Young⁶, Andrei S. Steindorff⁷, Stephen J. Mondo^{7,8}, Igor V. Grigoriev^{7,9},
6 Asaf Salamov⁷, Thomas Borch^{1,3,10}, Michael J. Wilkins^{1*}

7 * Corresponding author:

8 ¹Department of Soil and Crop Sciences, Colorado State University, Fort Collins, CO, USA

9 ²Rocky Mountain Research Station, U.S. Forest Service, Fort Collins, CO, USA

10 ³Department of Chemistry, Colorado State University, Fort Collins, CO, USA

11 ⁴Environmental Molecular Sciences Laboratory, Pacific Northwest National Laboratory, Richland, WA, USA

12 ⁵Department of Plant Pathology, University of California, Davis, CA, USA

13 ⁶Chemical Analysis & Instrumentation Laboratory, New Mexico State University, Las Cruces, NM, USA

14 ⁷Department of Energy Joint Genome Institute, Lawrence Berkeley National Laboratory, Berkeley, CA, USA

15 ⁸Department of Agricultural Biology, Colorado State University, Fort Collins, CO, USA

16 ⁹Department of Plant and Microbial Biology, University of California Berkeley, Berkeley, CA, USA

17 ¹⁰Department of Civil and Environmental Engineering, Colorado State University, Fort Collins, CO, USA

18

19 **Abstract**

20 **Warming climate has increased the frequency and size of high severity wildfires in the western**
21 **United States, with deleterious impacts on forest ecosystem resilience. Although forest soil**
22 **microbiomes provide a myriad of ecosystem functions, little is known regarding the impact of high**
23 **severity fire on microbially-mediated processes. Here, we characterized functional shifts in the soil**
24 **microbiome (bacterial, fungal, and viral) across wildfire burn severity gradients one year post-fire**
25 **in coniferous forests (Colorado and Wyoming, USA). We generated the Fire Responding**
26 **Ecogenomic database (FiRE-db), consisting of 637 metagenome-assembled bacterial genomes,**
27 **2490 viral populations, and 2 fungal genomes complemented by 12 metatranscriptomes from soils**
28 **affected by low and high-severity, and complementary marker gene sequencing and metabolomics**
29 **data. Actinobacteria dominated the fraction of enriched and active taxa across burned soils. Taxa**
30 **within surficial soils impacted by high severity wildfire exhibited traits including heat resistance,**
31 **sporulation and fast growth that enhanced post-fire survival. Carbon cycling within this system**
32 **was predicted to be influenced by microbial processing of pyrogenic compounds and turnover of**
33 **dominant bacterial community members by abundant viruses. These genome-resolved analyses**
34 **across trophic levels reveal the complexity of post-fire soil microbiome activity and offer**
35 **opportunities for restoration strategies that specifically target these communities.**

36

37

38 Introduction

39 Changes in climate coupled with the effects of long-term fire suppression and shifting land use
40 patterns have increased the frequency, severity, and season length of wildfires in the western US<sup>1-
41 4</sup>. In 2020 and 2021, much of the western US experienced severe wildfires of record-breaking
42 extent². High severity wildfires cause increased erosion⁵, elevated soil carbon (C) and nitrogen (N)
43 losses⁶, and subsequent nutrient and sediment export in stream water^{7,8}, so the increased
44 occurrence of severe wildfires may have important consequences for both terrestrial and aquatic
45 ecosystems. Shifting wildfire patterns have also been linked to slow post-fire revegetation and tree
46 seedling recruitment⁹ and thus delayed watershed recovery¹⁰⁻¹² in western US forests. **Although**
47 **ecosystem recovery from severe wildfires is closely linked to belowground biological processes,**
48 **little is known about the impact of high severity fire on soil microbiome function.**

49
50 **The soil microbiome regulates soil organic matter (SOM) decomposition and stabilization¹³, soil**
51 **nutrient dynamics¹⁴, and rhizosphere function¹⁵.** During severe wildfires, the soil microbiome can
52 be impacted directly due to heating killing heat-sensitive microbial taxa or indirectly via lasting
53 changes in soil chemistry (e.g., pH, organic matter structure) that continue to influence soil
54 microbiome assembly¹⁶. Wildfires reduce soil microbial community diversity in numerous
55 ecosystems¹⁷⁻²⁰ and such changes are likely to influence and potentially inhibit post-fire plant
56 recovery^{21,22}.

57
58 Although post-fire shifts in soil microbiome composition are relatively well characterized across
59 ecosystems^{16,18,19,23}, the impacts of fire on microbiome metabolic function and microbially-
60 mediated biogeochemical processes are not. To date, the vast majority of soil microbiome studies
61 following wildfire have measured ‘*who is there?*’, rather than focusing on how these compositional
62 shifts affect microbial metabolic functions. While several studies have noted post-fire reductions
63 in genes associated with N-cycling, carbohydrate metabolism, and methanogenesis^{24,25}, critical
64 knowledge gaps still exist regarding variability in microbiome responses among and within
65 wildfires due to differences in fire severity (i.e., the degree of vegetation and organic soil horizon
66 combustion). Such information is critical to understanding potential shifts in post-fire ecosystem
67 resilience and to guiding restoration approaches and omics tools have the potential to address this
68 key knowledge gap.

69
70 **Here, we studied burn severity gradients in two recent forest wildfires in Colorado and Wyoming**
71 **(USA). Soils were interrogated using a multi-omics approach to characterize how fire severity**
72 **influences C composition and the intimately connected soil bacterial, fungal, and viral**
73 **communities.** We hypothesized that higher severity wildfire would result in an increasingly altered
74 soil microbiome and that soil microbiomes colonizing burned soils would encode functional traits
75 (e.g., the capacity to utilize fire-altered substrates and rapidly recolonize vacant soil niches) that
76 favor the persistence of specific microbial taxa. Our analysis advances the understanding of
77 specific links between the soil microbiome and post-fire biogeochemical processes associated with

78 forest recovery and provides information critical to land and watershed managers tasked with
79 maintaining the desired ecosystem conditions and the sustained supply of ecosystem services.

80

81 **Methods**

82 *Field campaign*

83 Sampling was conducted in lodgepole pine (*Pinus contorta*) forests burned by Badger Creek (8215
84 ha) and Ryan (11567 ha) fires during 2018 in the Medicine Bow National Forest. Four candidate
85 burn severity gradients were selected based on US Forest Service, Burned Area Emergency
86 Response program (BAER) remotely sensed imagery and maps, and subsequently field
87 validated^{26,27}. Aspect, slope, and elevation were recorded at each sampling plot. Each gradient
88 comprised low, moderate, and high severity sites and an unburned control. Low, moderate, and
89 high severity sites had >85%, 20-85%, and <20% surficial organic matter cover, respectively²⁶.
90 Samples were collected on August 16 and 19 of 2019, approximately one year following
91 containment of both fires. At each sampling site, a 3 m x 5 m sampling grid with six m² subplots
92 was laid out perpendicular to the dominant slope (**Figure S1**). Subsamples of the organic soil
93 horizon (i.e., litter and duff; O-horizon) and upper mineral soil horizon (0-5 cm; A-horizon) were
94 collected with a sterilized trowel in each subplot for DNA and RNA extractions and subsequent
95 microbial analyses. In three subplots, additional material was collected for chemical analyses.
96 Samples for RNA analyses were immediately flash-frozen using an ethanol-dry ice bath and
97 subsequently placed on ice to remain frozen in the field. Samples for DNA extractions and
98 chemical analyses were immediately placed on ice and all samples were transported to the
99 laboratory at Colorado State University (CSU). Soils for DNA and RNA extractions were stored
100 at -80°C in the laboratory until processing. A total of 176 soil samples were collected
101 (**Supplementary data 1**).

102

103 *Soil chemistry*

104 We measured inorganic forms of soil N (NO₃-N and NH₄-N) in both organic and upper mineral
105 soils. Ten-gram subsamples were extracted with 50 mL of 2 M KCl within 24 h of sampling and
106 analyzed for NO₃-N and NH₄-N by colorimetric spectrophotometry²⁸ (Lachat Company,
107 Loveland, CO). A second subsample was oven dried at 105°C for 24 h to determine soil moisture
108 content. (**Supplementary data 1**).

109

110 *High-resolution carbon analyses: FTICR-MS*

111 Water extractions were completed on a subset of 47 samples from the Ryan Fire for high-resolution
112 C analyses using Fourier Transform Ion Cyclotron Resonance Mass Spectrometry (FTICR-MS) to
113 analyze dissolved organic matter (DOM) pools. Briefly, 100 mL of milliQ water was added to 50
114 g of sample in an acid-washed and combusted 250 mL Erlenmeyer flask. These were placed on a
115 shaker table for 10 hours at 170 rpm. Following shaking, liquid was poured off into a 50 mL
116 centrifuge tube and centrifuged for 10 min at 7500 g and supernatant was filtered through a
117 polypropylene 0.2 µm filter (polypropylene material). The extracts were acidified to pH 2 and

118 additionally pre-treated with solid-phase extractions using Agilent Bond Elut-PPL 3 mL columns
119 and diluted to 50 ppm (Agilent Technologies, DE, USA) following standard lab protocol²⁹. A 12
120 Tesla (12T) Bruker Solarix FTICR-MS located at the Environmental Molecular Sciences
121 Laboratory in Richland, WA, USA was used to collect DOM high-resolution mass spectra from
122 each DOM sample. Samples were directly injected into the instrument using a custom automated
123 direction infusion cart that performed two offline blanks between each sample and using an Apollo
124 II electrospray ionization (ESI) source in negative ion mode with an applied voltage of -4.2kV.
125 Ion accumulation time was optimized between 50 and 80 ms. One hundred and forty-four
126 transients were co-added into a 4MWord time domain (transient length of 1.1 s) with a spectral
127 mass window of m/z 100-900, yielding a resolution at m/z 400. Spectra were internally
128 recalibrated in the mass domain using homologous series separated by 14 Da (CH₂ groups). The
129 mass measurement accuracy was typically within 1 ppm for singly charged ions across a broad
130 m/z range (100 m/z - 900 m/z). Bruker Daltonics DataAnalysis (version 4.2) was used to convert
131 mass spectra to a list of m/z values by applying the FTMS peak picking module with a signal-to-
132 noise ratio (S/N) threshold set to 7 and absolute intensity threshold to the default value of 100.
133 Chemical formulae were assigned with Formularity³⁰ based on mass measurement error < 0.5 ppm,
134 taking into consideration the presence of C, H, O, N, S and P and excluding other elements. This
135 in-house software was also used to align peaks with a 0.5 ppm threshold. The R package
136 *ftmsRanalysis*^{31,32} was then used to remove peaks that either were outside the desired m/z range
137 (200 m/z – 900 m/z) or had an isotopic signature, calculate nominal oxidation state of carbon
138 (NOSC), and assign Van Krevelen compound classes. Raw FTICR-MS data is provided in archive
139 (doi:10.5281/zenodo.5182305).

140
141 Kendrick mass defect (KMD) analysis and plots were employed to identify potential increasing
142 polyaromaticity across the burn severity gradient. The KMD analysis was done using the C₄H₂
143 base unit (50 amu) to represent the addition of benzene to a separate molecular benzene. The mass
144 of each identified ion (M) was converted to its Kendrick mass (KM):

$$145 \quad \text{KM} = \text{M} * (50 \text{ amu} / 50.0587 \text{ amu}) \quad (1)$$

146
147
148 with 50 amu being the nominal mass of C₄H₂ and 50.0587 being the exact mass of C₄H₂. The final
149 KMD was obtained by subtracting the KM from the nominal KM, which is the initial ion mass
150 rounded to the nearest integer. Series were identified as 2 or more formulas with the same KMD
151 and a nominal Kendrick mass (NKM) differing by the C₄H₂ base unit (50 g/mol). Series were
152 retained if they were present across all four burn severity conditions (control, low, moderate, and
153 high), resulting in 64 total series in the final analysis.

154
155 *DNA extraction, 16S rRNA gene and ITS amplicon sequencing*

156 Total DNA was extracted from soil samples using the Zymobiomics Quick-DNA Fecal/Soil
157 Microbe Kits (Zymo Research, CA, USA). 16S rRNA genes in extracted DNA were amplified and

158 sequenced at Argonne National Laboratory on the Illumina MiSeq using 251-bp paired-end reads
159 and the Earth Microbiome Project primers 515F/806R³³, which targets the V4 region of the 16S
160 rRNA gene. To characterize fungal community composition, the DNA was also PCR amplified
161 targeting the first nuclear ribosomal internal transcribed spacer region (ITS) using the primers
162 (ITS1f/ITS2) and sequenced on the Illumina MiSeq platform at the University of Colorado
163 BioFrontiers Institute Next-Gen Sequencing Core Facility using 251-bp paired-end reads.

164

165 For taxonomic assignment, we used the SILVA³⁴ (release 132) and UNITE³⁵ (v8.3) databases for
166 bacteria and fungi, respectively. All sets of reads were clustered into amplicon sequence variant
167 (ASV) classifications using the QIIME2 pipeline³⁶ (release 2018.11). 16S rRNA gene and ITS
168 amplicon sequencing data discussed here is available at NCBI under BioProject #PRJNA682830.
169 Ecological guilds were assigned to fungal ASVs using FUNGuild³⁷ (v1.2). Guilds were
170 summarized into ‘Saprotroph’, ‘Ectomycorrhizal’, ‘Endophyte’, ‘Epiphyte’, and ‘Arbuscular
171 mycorrhizal’, and were only retained if the confidence ranking was ‘probable’ or ‘highly
172 probable’. If a taxon was classified as multiple guilds that were not consistent in the main guilds
173 listed above (e.g., saprotroph), it was not used for downstream analysis. For example, an ASV
174 classified as ‘Animal Pathogen-Endophyte-Wood Saprotroph’ would not be retained but an ASV
175 classified as ‘Wood Saprotroph-Soil Saprotroph’ would be retained and renamed ‘Saprotroph’.

176

177 To characterize how microbial populations differed across burn severities and soil horizons, we
178 used the R³⁸ *vegan*³⁹ (v2.5-7) and *phyloseq*⁴⁰ (v1.28.0) packages. Nonmetric multidimensional
179 scaling (NMDS) was used to examine broad differences between microbial communities. Analyses
180 of similarity (*vegan::anosim*) was additionally utilized to statistically test the magnitude of
181 dissimilarity between microbial communities from the different burn severity conditions and soil
182 horizons. Mean species diversity of each sample (alpha diversity) was calculated based on species
183 abundance, evenness, or phylogenetic relationships using Shannon’s Diversity Index (H), Faith’s
184 Phylogenetic Diversity (pd), and Pielou’s Evenness (J). Linear discriminant analysis (LDA) with
185 a score threshold of 2.0 was used to determine ASVs discriminant for unburned or burned soil⁴¹.

186

187 *Metagenomic assembly and binning*

188 A subset of 12 Ryan Fire samples from a single transect representing low and high severity burn
189 from organic and mineral horizon soils was selected for metagenomic sequencing to analyze
190 changes in microbial community functional potential (n=3 per condition). ANOSIM analyses of
191 16S rRNA gene data confirmed that the soil microbial communities were not significantly different
192 between the Ryan and Badger Creek sites ($R = 0.09$, $p < 0.05$), so we focused on the Ryan Fire as
193 a representative site. The different conditions are hereafter referred to as ‘Low O’ (low severity
194 organic horizon), ‘High O’ (high severity organic horizon), ‘Low A’ (low severity mineral
195 horizon), and ‘High A’ (high severity mineral horizon). Libraries were prepared using the Tecan
196 Ovation Ultralow System V2 and were sequenced on the NovaSEQ6000 platform on a S4 flow
197 cell using 151-bp paired-end reads at Genomics Shared Resource, Colorado Cancer Center,

198 Denver, CO, USA. Sequencing adapter sequences were removed from raw reads using BBduk
199 (<https://jgi.doe.gov/data-and-tools/bbtools/bb-tools-user-guide/bbduk-guide/>) and reads were
200 trimmed with Sickle⁴² (v1.33). For each sample, trimmed reads were assembled into contiguous
201 sequences (contigs) using the de novo de Bruijn assembler MEGAHIT v1.2.9 using kmers⁴³
202 (minimum kmer of 27, maximum kmer of 127 with step of 10). Assembled contigs greater than
203 2500bp were binned using MetaBAT2 with default parameters⁴⁴ (v2.12). Metagenome-assembled
204 genome (MAG) quality was estimated using checkM⁴⁵ (v1.1.2) and taxonomy was assigned using
205 GTDB-Tk⁴⁶ (R05-RS95, v1.3.0). MAGs from all samples were combined and dereplicated using
206 dRep⁴⁷ (default parameters, v2.2.3) to create a non-redundant MAG database. Low quality MAGs
207 (<50% completion and >10% contamination) were excluded from further analysis⁴⁸. Reads from
208 all samples were mapped to the dereplicated bin database using BBMap with default parameters
209 (version 38.70, <https://sourceforge.net/projects/bbmap/>). Per-contig coverage across each sample
210 was calculated using CoverM contig (v 0.3.2) (<https://github.com/wwood/CoverM>) with the
211 ‘Trimmed Mean’ method, retaining only those mappings with minimum percent identity of 95%
212 and minimum alignment length of 75%. Coverages were scaled based on library size and scaled
213 per-contig coverages were used to calculate the mean per-bin coverage and relative abundance in
214 each sample (**Supplementary data 2**). The quality metrics and taxonomy of the subsequent 637
215 medium- and high-quality MAGs discussed here are included in the supplementary material
216 (**Supplementary data 3**) and are deposited at NCBI (BioProject ID PRJNA682830). Maximum
217 cell doubling times were calculated from codon usage bias (CUB) patterns in each MAG using
218 gRodon⁴⁹.

219

220 *Metagenome-assembled genome annotation*

221 Eukaryotic MAGs were annotated using the JGI Annotation Pipeline analyzed with
222 complementary metatranscriptomics assemblies⁵⁰ (RnaSPAdes, v3.13.0) and are deposited on
223 MycoCosm⁵¹ (<https://mycocosm.jgi.doe.gov>). Bacterial MAGs were annotated using DRAM⁵²
224 (v1.0). In addition to the DRAM annotations, we used HMMER⁵³ against Kofamscan HMMs⁵⁴ to
225 identify genes for catechol and protocatechuate meta- and ortho-cleavage, naphthalene
226 transformations, and inorganic N cycling (**Supplementary data 4**). A metabolic pathway within
227 a MAG is considered complete if it is $\geq 50\%$ complete because MAGs are commonly not 100%
228 complete.

229

230 *Metatranscriptomics*

231 Total RNA was extracted from the subset of 12 samples utilized for metagenomics using the
232 Zymobiomics DNA/RNA Mini Kit (Zymo Research, CA, USA) and RNA was cleaned, DNase
233 treated, and concentrated using the Zymobiomics RNA Clean & Concentrator Kit (Zymo
234 Research, CA, USA). Ribosomal RNA was removed from total RNA and libraries were prepared
235 using the Takara SMARTer Stranded Total RNA-Seq Kit v2 (Takara Bio Inc, Shiga, Japan).
236 Samples were sequenced on the NovaSEQ6000 platform on a S4 flow cell using 151-bp paired-
237 end reads at Genomics Shared Resource, Colorado Cancer Center, Denver, CO, USA. Adapter

238 sequences were removed from raw reads using Bbduk (<https://jgi.doe.gov/data-and->
239 [tools/bbtools/bb-tools-user-guide/bbduk-guide/](https://jgi.doe.gov/data-and-tools/bbtools/bb-tools-user-guide/bbduk-guide/)) and sequences were trimmed with Sickle v1.33⁴².
240 Trimmed reads were mapped to metagenome assemblies using BMap (parameters:
241 ambiguous=random, idfilter=0.95; v38.70). Mappings were filtered to 95% identity and counts
242 were generated using HTSeq⁵⁵. For broad analysis of differential expression, the dataset was
243 filtered to only transcripts which were successfully annotated by DRAM (n=146,895) and
244 DESeq2⁵⁶ was used to identify transcripts that were differentially expressed in either burn severity
245 within soil horizons (e.g., high vs. low in organic horizon soils and vice versa). The same analysis
246 was also run on the combined HMM output described above (1,189 total transcripts). We
247 normalized our dataset by calculating the gene length corrected trimmed mean of M values⁵⁷
248 (geTMM) using edgeR⁵⁸ to normalize for library depth and gene length. To identify transcripts
249 that were highly expressed in any given condition, we filtered the data to only transcripts that were
250 in the upper 20% of TMM for 2 of the 3 samples in any one condition (**Table S1**). To compare
251 bacterial and fungal expression data for individual genes, we normalized the number of either
252 fungal or bacterial transcript reads to the gene coverage in each sample to compare the number of
253 transcripts recruited per gene.

254

255 *Viruses*

256 **Viral contigs were recovered from the metagenomic assemblies using VirSorter2⁵⁹ (v2.2.2) and**
257 **only contigs ≥ 10 kb with a VirSorter2 score > 0.5 were retained.** Subsequent viral contigs were
258 trimmed using checkV⁶⁰ (v0.4.0) and the final contigs were clustered using the CyVerse app
259 ClusterGenomes (v1.1.3) requiring an average nucleotide identity of 95% or greater over at least
260 80% of the shortest contig. The final DNA viral metagenome-assembled genomes (vMAG) dataset
261 was manually curated using the checkV, VIRSorter2, and DRAM-v annotation outputs according
262 to standard protocol⁶¹. RNA vMAGs were also recovered from metatranscriptome assemblies
263 using VIRSorter2⁵⁹ (v2.2.2). The resulting sequences were clustered using ClusterGenomes
264 (v1.1.3) on CyVerse using the aforementioned parameters. To quantify relative abundance of DNA
265 and RNA vMAGs across the 12 samples, we mapped the metagenomic and metatranscriptomic
266 reads to the vMAGs using BMap with default parameters (v38.70). To determine vMAGs that
267 had reads mapped to at least 75% of the vMAG, we used CoverM (v0.6.0) in contig mode to find
268 vMAGs that passed this 75% threshold (--min-covered-fraction 75). We then used CoverM
269 (v0.6.0) in contig mode to output reads per base and used this to calculate final DNA and RNA
270 vMAG relative abundance in each metagenome and metatranscriptome. vConTACT2 (v0.9.8;
271 CyVerse) was used to determine vMAG taxonomy. Final viral sequences are deposited on NCBI
272 (BioProject ID #PRJNA682830 - BioSamples SAMN20555178, SAMN20555179;
273 **Supplementary data 5**). We used DRAM-v⁵² (v1.2.0) to identify auxiliary metabolic genes
274 (AMGs) within the final viral database⁵² (**Supplementary data 6**).

275

276 CRISPR-Cas protospacers were found and extracted from MAG sequences using the CRISPR
277 Recognition Tool⁶² (CRT, minimum of 3 spacers and 4 repeats) in Geneious (v2020.0.3) and

278 CRISPRASSEMBLER⁶³ with default parameters (v1.0.1). BLASTn was used to compare MAG
279 protospacer sequences with protospacer sequences in vMAGs with matches only retained if they
280 were 100% or contained ≤ 1 bp mismatch with an e-value $\leq 1e-5$. To identify putative vMAG-MAG
281 linkages, we used an oligonucleotide frequency dissimilarity measure (VirHostMatcher) and
282 retained only linkages with a d_2^* value < 0.25 ⁶⁴ (**Supplementary data 7**).

283

284 **Results & Discussion**

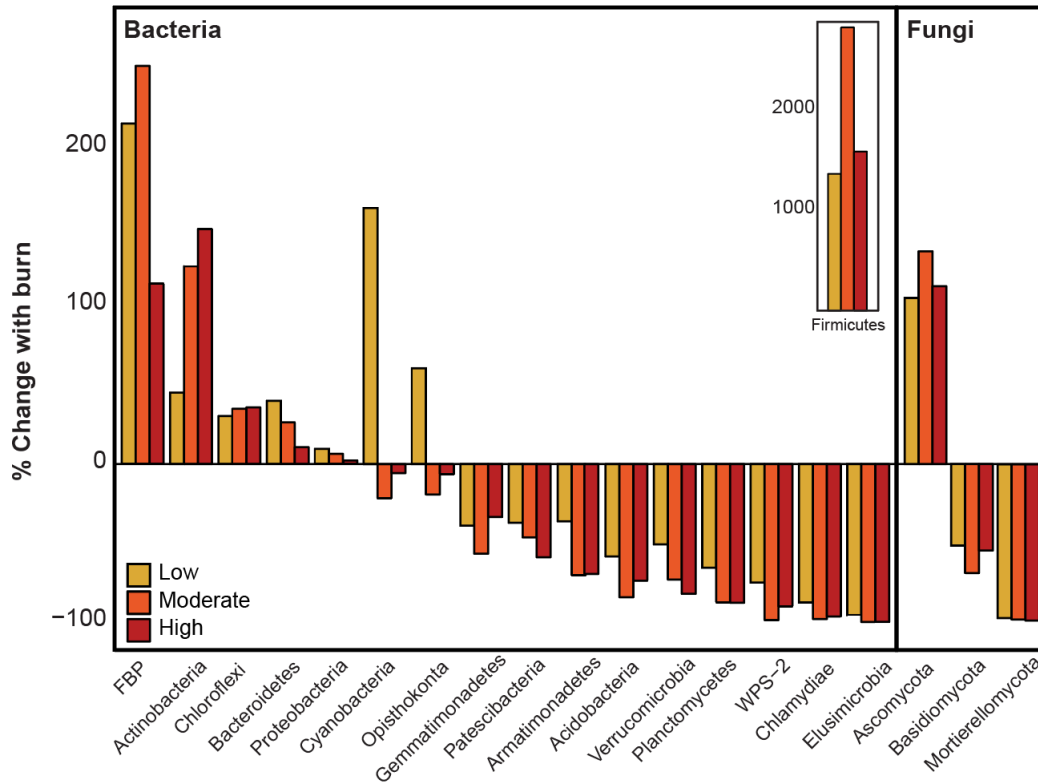
285 *Increasing fire severity drives decreasing diversity and compositional shifts in the soil*
286 *microbiome*

287 Near surface soils were collected approximately one year post-fire from four burn severity gradient
288 transects (control, low, moderate, and high burn severity) across two distinct wildfires that
289 occurred in 2018 along the Colorado-Wyoming border. Bacterial and fungal communities in all
290 samples were profiled using marker gene analyses, while a subset of twelve samples (soils
291 impacted by either low or high wildfire severity within the Ryan fire) were additionally
292 interrogated with metagenomic and metatranscriptomic sequencing. **Bacterial and fungal**
293 **communities within burned and unburned soils were significantly different (bacterial ANOSIM R**
294 **= 0.57, $p < 0.05$; fungal ANOSIM R = 0.72, $p < 0.05$) (Figure S2). Reflecting observations from**
295 **prior studies^{17,20,65,66}, bacterial communities in burned soils were characterized by lower diversity**
296 **and were enriched in Actinobacteria and Bacteroidetes relative to unburned controls (Figure 1).**
297 **Specifically, the Actinobacteria genera *Arthrobacter*, *Modestobacter*, *Blastococcus*, and**
298 ***Actinomadura* had the largest relative abundance increases in burned soils relative to control soils**
299 **and were discriminant features of these conditions (Supplementary data 8). The diversity of**
300 **fungal communities in surficial soils also decreased with fire (Figure 2E) and, similar to previous**
301 **studies^{18,67,68}, shifted from Basidiomycete- to Ascomycete-dominated with the Basidiomycota**
302 **relative abundance decreasing by ~58% (Figure 1). Discriminant fungal taxa included ASVs from**
303 **the *Sordariomycetes*, *Saccharomycetes*, and *Dothideomycetes*, taxa also found in previous fire**
304 **studies^{66,68} (Supplementary data 8).**

305

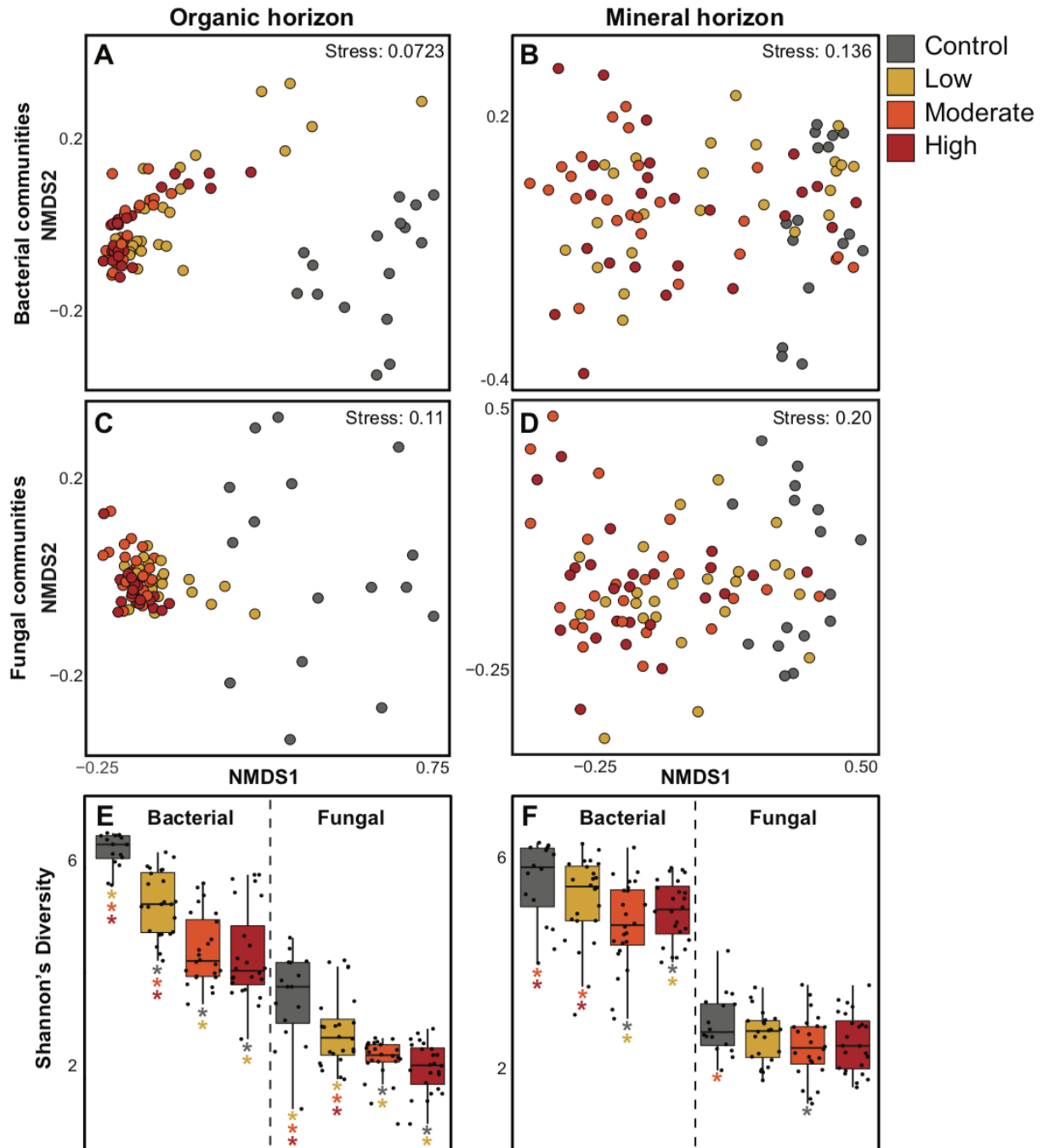
306 **While shifts in community composition between burned and control conditions were observed in**
307 **both organic and mineral soil horizons, the surficial organic layers changed more than the deeper**
308 **mineral horizon soil. Microbial diversity generally decreased with increasing fire severity in the**
309 **organic horizons, although differences between moderate and high severity were statistically**
310 **indistinct (Figure 2). Similarly, as fungal and bacterial diversity decreased with burn severity, beta**
311 **dispersion ('distance to centroid') calculations revealed increasingly similar microbial community**
312 **structures (Figure S3) with a less complex bacterial and fungal community structure (Table S2).**
313 **These shifts resulted in significant dissimilarity between microbial communities in organic**
314 **horizons impacted by either low or high severity wildfire (bacterial ANOSIM R=0.15, $p < 0.05$;**
315 **fungal ANOSIM R=0.25, $p < 0.05$). In contrast, mineral soils that were less impacted by wildfire**
316 **displayed an opposite effect, with increasing beta dispersion after wildfire that signifies greater**
317 **bacterial community dissimilarity (Figure S3). Stochastic community shifts in deeper soils may**

318 follow wildfire, potentially due to spatially heterogeneous changes in soil chemistry and nutrient
319 availability. Together, these data highlight the susceptibility of highly combustible surficial
320 organic soil horizons to wildfire, resulting in less diverse and inter-connected microbial
321 communities. In contrast, mineral soils are likely more insulated from the effects of fire, and
322 therefore the soil microbiome displays a more muted response to wildfire effects.
323
324
325



345

346 **Figure 1** The percent change in relative abundance from control to low, moderate, and high
347 severity in organic soil horizons of each main bacterial and fungal phylum. Phyla with relative
348 abundance less than 0.5% were discarded for this analysis. Note that although the *Firmicutes* have
349 the largest increase with burn (inset) their overall relative abundance is still low.
350
351
352
353
354



355
356

357 **Figure 2.** Non-metric multidimensional scaling (NMDS) of organic (A, C) and mineral soil
358 horizons (B, D) bacterial (A, B) and fungal (C, D) communities shows increased separation of
359 burned and unburned microbial communities in surficial organic horizon relative to deeper mineral
360 soil communities. Shannon's diversity (H) calculated from 16S rRNA and ITS gene sequencing in
361 organic (E) and mineral soil horizons (F) further shows the increased susceptibility of
362 microbiomes in organic horizons to wildfire.

363

364

365 *Development of a unique MAG database from fire-impacted soils.*

366 While a myriad of studies have reported changes in microbial community membership in response
367 to wildfire^{66,69–71}, the functional implications of these shifts are difficult to infer from marker gene
368 studies. Here we used genome-resolved metagenomics to generate the **Fire Responding**
369 **Ecogenomic database (FiRE-db)**, a comprehensive, publicly accessible database of fire-
370 responding bacterial, fungal, and viral genomes from coniferous forest soils (BioProject ID
371 #PRJNA682830). From metagenomics sequencing of 12 burned (low and high severity) forest soil
372 samples we reconstructed 637 medium- and high-quality bacterial metagenome assembled
373 genomes (MAGs) that reflected the majority of dominant taxa observed in complementary 16S
374 rRNA gene analyses (**Figure S4**). This database spans 21 phyla and encompasses 237 genomes
375 from taxa within the Actinobacteria, 167 from the Proteobacteria, 62 from the Bacteroidota, and
376 52 from the Patescibacteria. Furthermore, we recovered 2 fungal genomes from the Ascomycota,
377 which were affiliated with *Leotiomyces* and *Coniochaeta lignaria*. We additionally recovered
378 2,399 DNA and 91 distinct RNA vMAGs from the 12 metagenomes and metatranscriptomes
379 (**Table S5**).

380

381 *Actinobacteria respond strongly to high severity wildfire disturbances in surface soils.*

382 Reflecting observations from 16S rRNA gene analyses, MAGs affiliated with the Actinobacteria
383 genera *Blastococcus*, *Mycetocola*, *SISG01*, *SCTD01*, *Nocardiodes*, and *Arthrobacter* were all
384 enriched (relative to control soils) in surface organic soil horizons (O-horizon) impacted by high
385 severity wildfire (hereafter referred to as ‘High O’) that in most instances had been combusted to
386 an ash layer. Because of their enrichment following wildfire, we have focused on 8 featured
387 Actinobacteria MAGs (MAGs RYN_93, RYN_94, RYN_101, RYN_124, RYN_147, RYN_169,
388 RYN_175, RYN_216) for analyses described below. Combined, these MAGs accounted for an
389 average relative abundance of 19% in High O soils and 12% in O-horizon soils impacted by low
390 severity wildfire (‘Low O’ soils). Furthermore, metatranscriptomic analyses indicated that these
391 MAGs were also among the most active in High O samples, accounting for an average of nearly
392 4% of gene expression across samples. These MAGs were also active in Low O samples, but to a
393 lesser extent (accounting for 1.5% of expression). Together, all 237 Actinobacteria MAGs were
394 responsible for ~51% of gene expression in the High O soils and ~42% in Low O samples.

395

396 High severity wildfire exerts a pulse disturbance on surficial organic soil horizons by exposing
397 them to high heat. Thus, the taxa that constitute the post-fire microbiome and fill new niches in
398 the soil likely encode traits for thermal resistance. Nearly all the aforementioned Actinobacterial
399 MAGs encoded sporulation genes, indicating that spore formation is likely a key strategy to ensure
400 survival and colonization post-fire (**Figure 3A**). These MAGs also all contained genes encoding
401 heat shock proteins and molecular chaperones which may further facilitate thermal resistance
402 (**Figure 3A**). In the majority of these MAGs, thermal resistance was complimented by genes for
403 mycothiol biosynthesis, a compound produced by Actinobacteria that aids in oxidative stress

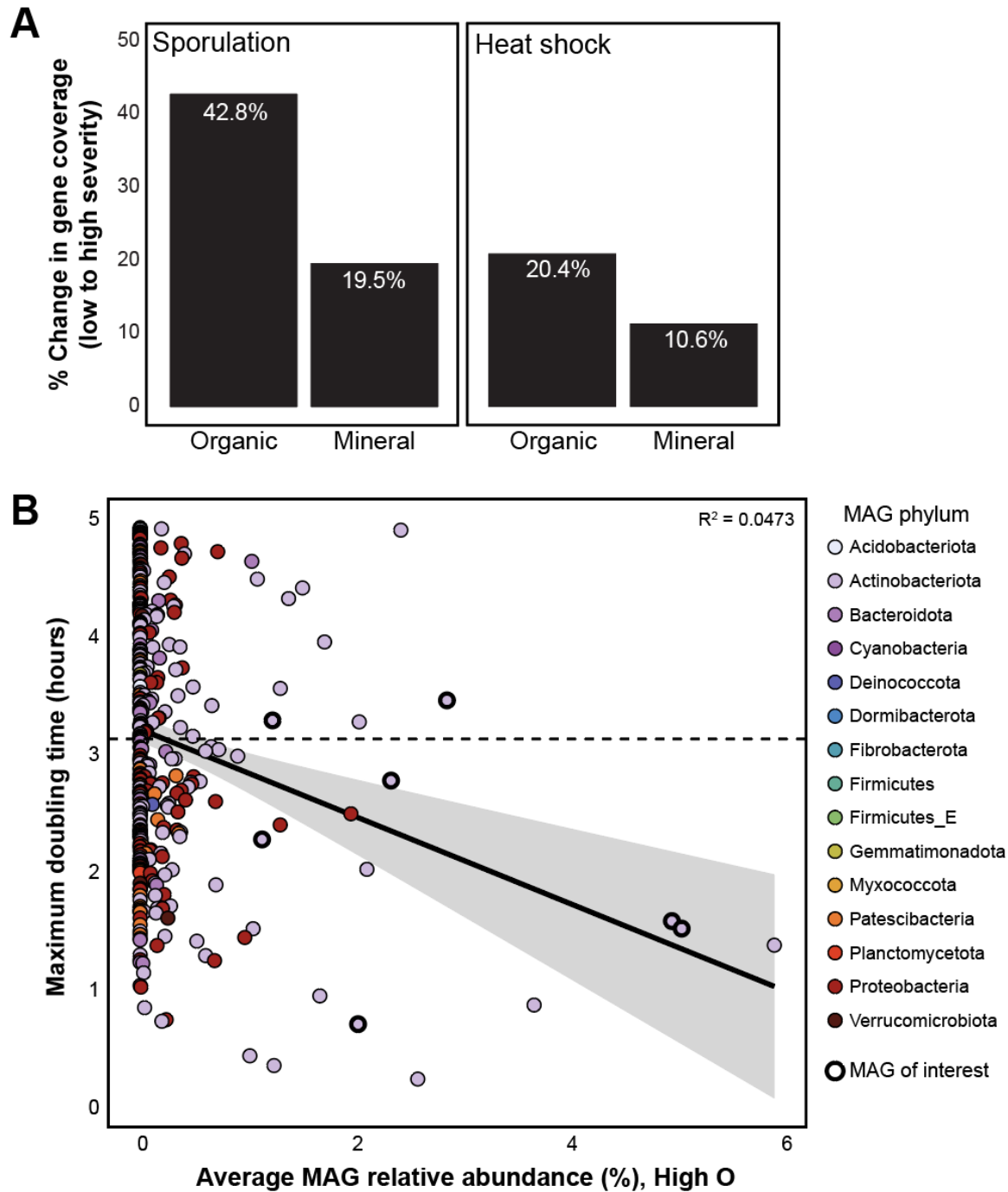
404 tolerance⁷². Finally, MAG RYN_93 encoded *ectB* for synthesizing ectoine, a compatible solute for
405 environmental stress tolerance⁷³. In general, MAGs recovered from High O samples also had
406 significantly higher GC content than MAGs from mineral soil layers (e.g., A horizons) impacted
407 by low ('Low A') and high ('High A') wildfire severity (**Figure S5**). Higher GC content may be
408 another heat resistance trait due to the thermal stability of the GC base pair^{74,75}. The heating of
409 organic soil horizons during wildfire lyses heat-sensitive microorganisms, resulting in an influx of
410 labile organic C and N associated with necromass⁷⁶. This likely opens up niche space to fire-
411 resistant heterotrophic taxa and stimulates growth rates of these taxa⁷⁷. Each of the abundant
412 featured Actinobacteria MAGs expressed peptidase genes (88 total genes) in High O samples, of
413 which approximately twenty were differentially expressed ($p < 0.05$) between High O and Low O
414 conditions. These included genes responsible for the degradation of peptidoglycan (component of
415 bacterial cell walls) and chitin (component of fungal cell walls), suggesting that taxa enriched post-
416 fire actively utilize microbial necromass.

417
418 The ability to grow quickly and occupy available niches in the environment is likely a key trait for
419 microorganisms colonizing burned soils^{66,78}. We inferred maximum growth rates across our
420 bacterial MAGs to determine whether colonizing taxa encoded the potential for rapid growth in
421 burned soils⁴⁹. Potential growth rates (as maximum cell doubling times) were calculated from
422 patterns of codon usage bias (CUB) in each MAG^{79,80}. After removal of all MAGs with doubling
423 time greater than 5 hours due to model inaccuracies at slower growth rates⁴⁹, the average doubling
424 time within our MAG database was 3.16 hours. All but two of the dominant MAGs in High O
425 samples had doubling times faster than the database average (ranging from 0.73 to 3.59 hours)
426 (**Figure 3B**). These insights suggest that abundant bacteria sampled one year post-wildfire likely
427 occupied niches in the immediate aftermath of wildfire through rapid cell growth. In contrast, these
428 patterns were absent from MAGs from High A soils (**Figure S7**). Emphasizing the importance of
429 fast growth for colonizing severely burned soils, only 19 bacterial MAGs from High O samples
430 had growth rates too slow for the model to accurately estimate (total of 249 MAGs with growth
431 rates > 5 hours). To determine whether these same microorganisms were growing rapidly at the
432 time of sampling (one year post-wildfire), we investigated gene expression associated with rapid
433 growth (i.e., ribosomes, central metabolism) through MAG abundance-normalized transcripts.
434 Results suggested diminished growth rates for the dominant High O MAGs at time of sampling,
435 relative to other Actinobacteria MAGs (e.g., *Blastococcus*, *Nocardiodes*) that accounted for high
436 expression of ribosomal genes and components of the TCA cycle in High O samples. Together,
437 these analyses indicate that the rapid growth rates enabling 'fast-responders' to occupy free niche
438 space in soil immediately following wildfire are not maintained once those niches are filled.

439
440
441
442
443

444

445



455 **Figure 3.** (A) Genes encoding for heat resistant traits (sporulation and heat shock) increase in
456 coverage from low to high severity conditions in the organic and mineral soil horizon
457 metagenomes, but to a lesser degree in the mineral horizon soils. (B) The MAGs of interest that
458 are enriched and highly active in High O generally have a faster growth rate (lower maximum

459 doubling time, estimated using gRodon⁴⁹) than the average growth rate (indicated here with the
460 dashed line) in our MAG database.

461

462 *Deeper burned soils are dominated by distinct microbial membership*

463 High A soils hosted a greater diversity of enriched and active MAGs relative to the overlying
464 organic soil horizons. Actinobacteria again contributed strongly to these signals, with the
465 dominant, active MAGs in the mineral horizons affiliated with the families *Streptosporangiaceae*,
466 *Solirubrobacteraceae*, *Frankiaceae*, and *Streptomycetaceae* (MAGs RYN_173, RYN_225,
467 RYN_228, RYN_220, RYN_230, RYN_265). Additional highly abundant and active MAGs in
468 High A samples were affiliated with the Eremiobacterota, Dormibacterota, and Proteobacteria
469 phyla (MAGs RYN_132, RYN_309, RYN_342, RYN_347, RYN_607). Together, these MAGs
470 accounted for ~20% of the High A community composition, and nearly 14% of total MAG gene
471 expression. These MAGs were also active in Low A soils, albeit to a lesser extent (accounting for
472 ~5% of total expression).

473

474 Genes associated with thermal resistance were again common in the dominant High A MAGs.
475 Three of the MAGs discussed here (RYN_220, RYN_225, RYN_342) had metabolic potential to
476 synthesize the environmental stress protectant mycothiol⁷². The second most active MAG in High
477 A samples (RYN_220) was affiliated with the *Streptomyces* which have been shown to form
478 sporogenic structures (aerial hyphae) in response to adverse conditions (i.e., high temperatures,
479 nutrient depletion)⁸¹. We observed an overall increase in spore-forming gene coverage from Low
480 A to High A conditions (**Figure 2A**) and all MAGs discussed here encoded at least one sporulation
481 gene. Additionally, members of *Streptomyces* are known for their ability to scavenge nutrients and
482 utilize a diverse array of organic substrates⁸², which is evidenced here through expression of
483 abundant and diverse CAZymes that are predicted to target chitin, polyphenolics, and pectin,
484 among other substrates (**Figure S6**).

485

486 Associated with the enrichment and activity of *Streptomyces* in High A soils, we observed high
487 expression of genes encoding the biosynthesis of cobalamin (vitamin B12, *cob* genes). Cobalamin
488 production is conserved within a relatively small group of microorganisms – including
489 *Streptomyces* – and can serve as a keystone function within ecosystems⁸³. The entire aerobic
490 cobalamin biosynthesis pathway was expressed in Low A and High A samples (**Figure S8**;
491 pathway adapted^{83,84}). Here, a *Streptomyces* MAG (RYN_220) was responsible for 12% of MAG
492 gene expression linked to cobalamin biosynthesis in High A soils. In total, the MAGs mentioned
493 above were responsible for nearly 90% of the total cobalamin biosynthesis MAG gene expression
494 in High A samples. These observations contrast directly with High O samples; the general absence
495 of *Streptomyces* in these samples resulted in limited expression of this pathway. Cobalamin
496 biosynthesis gene expression was ~175% greater in High A samples, and 3 of the aforementioned
497 MAGs (RYN_342, RYN_225, RYN_220, RYN_347) differentially expressed *cobB*, *cobA/O*, and
498 *btuB* (cobalamin transporter gene) in High A soils relative to High O. In the A-horizon, the

499 increased transcription of genes for cobalamin synthesis is likely a beneficial consequence of
500 wildfire enriching taxa that encode this trait (i.e., *Streptomyces*). Given the noted importance of
501 this cofactor in mediating a range of critical soil microbiome functions, this process could
502 potentially aid in plant reestablishment⁸⁵, enhance ecosystem function across trophic levels⁸⁶, and
503 thus be beneficial for the overall restoration of post-fire landscapes.

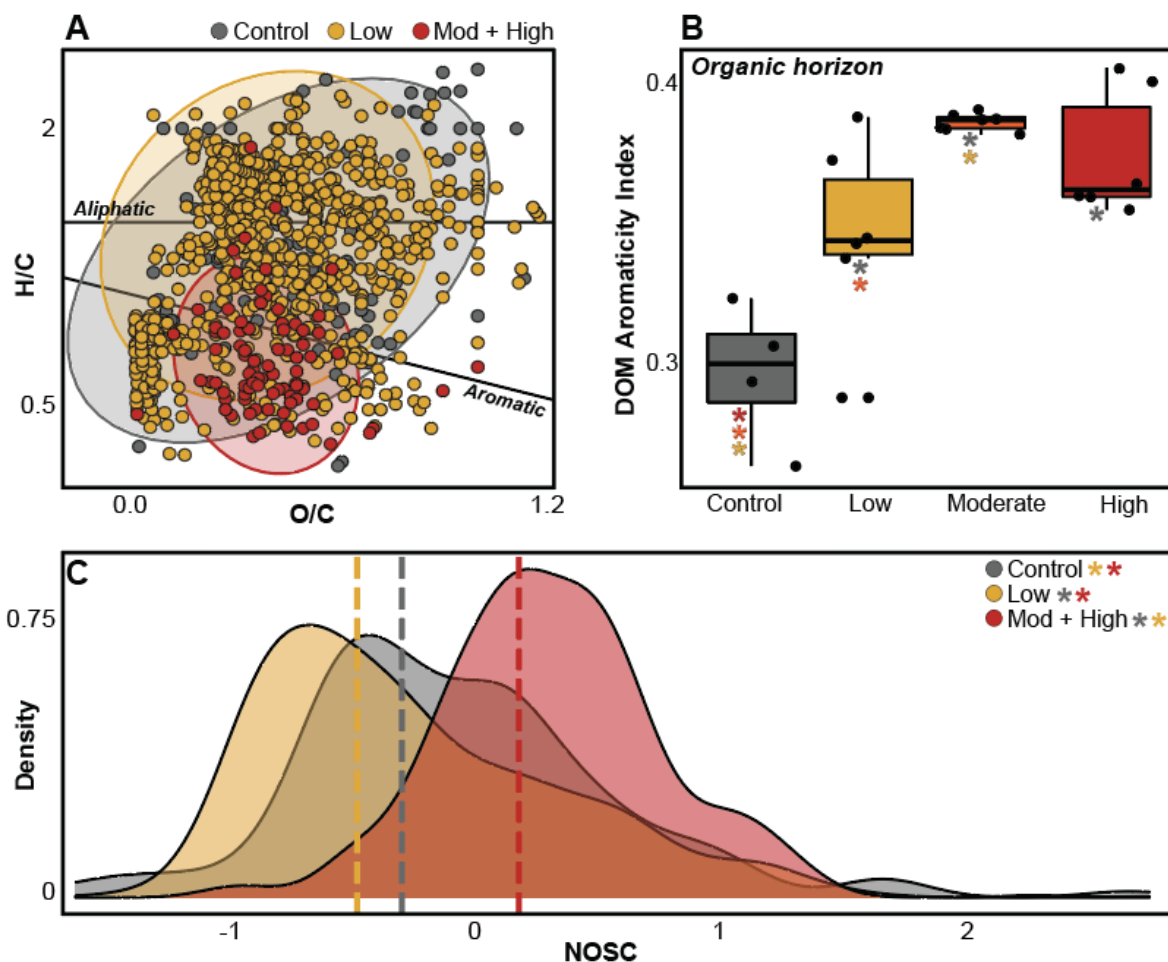
504

505 *Actinobacteria catalyze degradation of pyrogenic organic matter*

506 During wildfire, SOM may be transformed to increasingly aromatic molecular structures that are
507 commonly considered less labile for microbial utilization⁸⁷. Mass spectrometry DOM analyses
508 found evidence for increasing aromaticity with burn severity in organic horizon soils (**Figure 4**).
509 Low severity wildfire drives an increase in DOM aromaticity (**Figure 4B**) but also an
510 accumulation of other unique compounds likely resulting from incomplete combustion of SOM⁸⁸
511 (**Figure 4A**). In contrast, the unique compounds formed following moderate and high severity
512 wildfire were constrained to the aromatic region (**Figure 4A**). Reflecting the more insulated,
513 deeper mineral soils, these aromaticity index trends were not identified in DOM released from
514 mineral horizons (**Figure S9**). To estimate lability of these DOM pools, we calculated NOSC
515 which can reveal the potential thermodynamic favorability of a carbon substrate, with higher
516 NOSC values theoretically yielding a lower $\Delta G_{C_{ox}}$ (i.e., more favorable) when coupled to the
517 reduction of an electron acceptor⁸⁹. Unique formulas detected in High O samples had significantly
518 higher NOSC values than both Low O and control samples, indicating increasing thermodynamic
519 favorability of DOM following severe wildfire (**Figure 4C**).

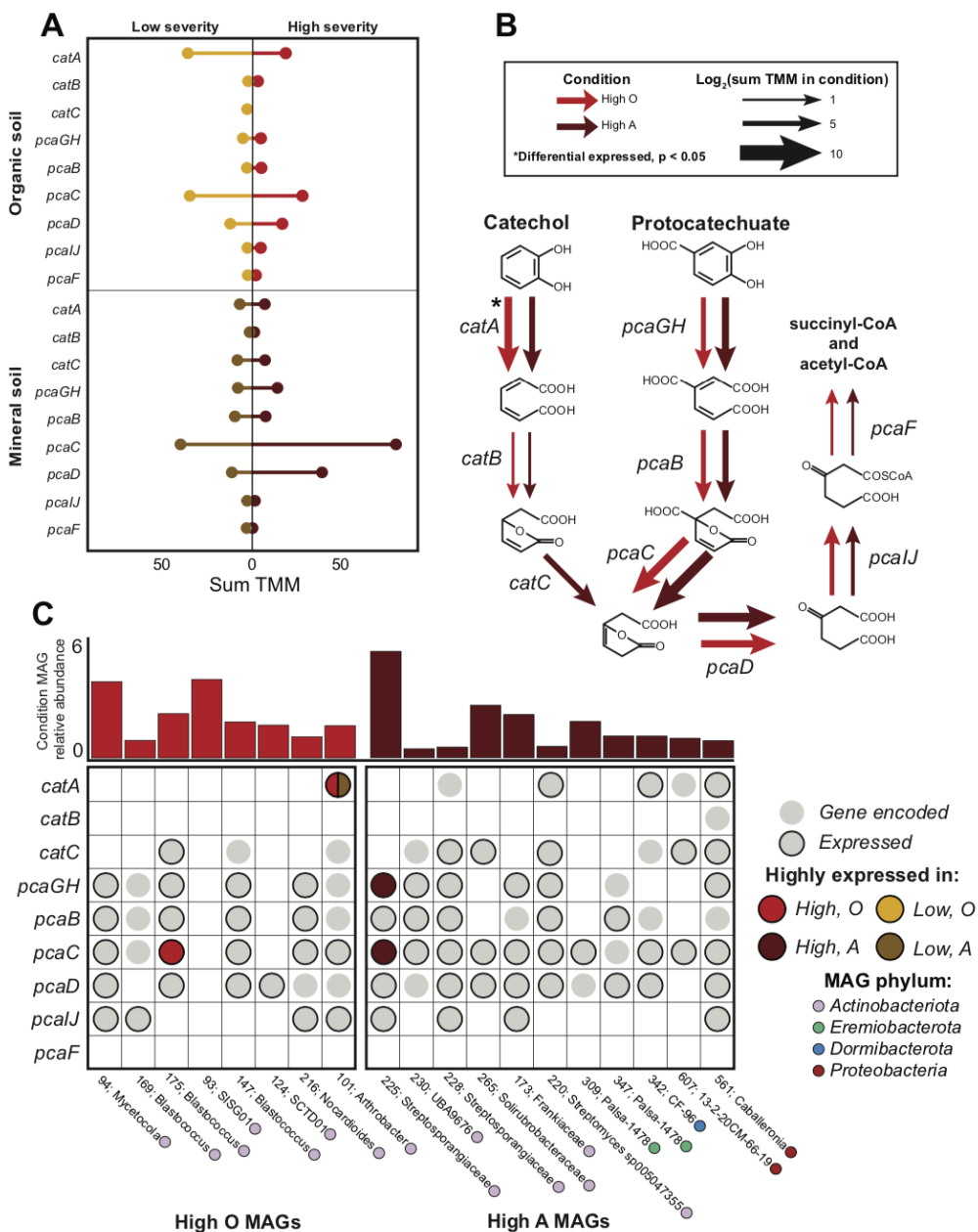
520

521 **Wildfire severity-driven chemical changes likely mediate the extent of microbial DOM processing.**
522 **We focused on the ability of community members to process catechol and protocatechuate, the**
523 **two intermediate products formed during aerobic degradation of diverse aromatic compounds⁹⁰.**
524 **The genomic potential for these reactions was broadly distributed across burn severities and was**
525 **dominated by Actinobacteria and Proteobacteria (**Figure 5**); 80 and 226 MAGs encoded at least**
526 **50% of the catechol and protocatechuate ortho-cleavage pathways, respectively, including most of**
527 **the featured High O and High A MAGs (**Figure 5C**).** Meta-cleavage pathways were also broadly
528 represented within the MAG database (**Figure S10**). There was additional evidence for activity of
529 both pathways regardless of soil horizon and wildfire severity (**Figure 5A**). In High O samples,
530 the *Arthrobacter* MAG RYN_101 alone was responsible for ~44% of *catA* (catechol 1,2-
531 dioxygenase) gene expression, and therefore likely plays a key role in catechol degradation.
532 Contrastingly, in High A samples, the *Streptosporangiaceae* MAG RYN_225 was responsible for
533 ~46% and 23% of the expression of *pcaGH* (protocatechuate 3,4-dioxygenase) and *pcaC* (4-
534 carboxymuconolactone decarboxylase) that catalyzes protocatechuate degradation (**Figure 5C**).
535 However, none of the dominant MAGs across High O and High A samples encoded the entire
536 catechol or protocatechuate ortho-cleavage pathway (**Figure 5C**), indicating that metabolic
537 handoffs between community members are likely important for complete degradation of these
538 compounds.



539
540 **Figure 4.** (A) Van Krevelen diagram showing unique formulas from organic soil horizons in
541 unburned, low, and moderate and high (combined) organic soil horizons. (B) Aromaticity index of
542 DOM pools extracted from organic soil horizons across the burn severity gradient. Colored
543 asterisks indicate significant difference between the two conditions ($p < 0.05$). (C) Density plot of
544 unique formula NOSC value distributions between different conditions. Dashed lines show NOSC
545 medians for each condition.

546
547
548
549
550
551
552
553
554



585

586 **Figure 5. (A)** The summed TMM of each gene for catechol and protocatechuate ortho-cleavage in
 587 each condition. **(B)** The pathway for catechol and protocatechuate ortho-cleavage with arrows
 588 indicating the log normalized sum TMM of the gene for high severity organic and mineral soil
 589 horizons. Asterisks indicate genes that are differentially expressed in the condition (p<0.05). **(C)**
 590 The genomic potential and expression of each gene in the pathway for the MAGs enriched and
 591 active in high severity organic and mineral soil samples. The above bar chart shows the featured
 592 MAG relative abundance in that condition, colored by featured condition.

593

594

595 *Viral dynamics impact community structure and function of the burned soil microbiome*

596 We recovered 2399 distinct DNA viral populations and 91 distinct RNA viral populations
597 (vMAGs) from the metagenomic and metatranscriptomic assemblies. Highlighting the viral
598 novelty in these ecosystems, 945 of the DNA and RNA vMAGs were previously undescribed (only
599 clustering with other vMAGs from this study) and 92 were given taxonomic assignments, with the
600 majority (n=86) within the *Caudovirales* order (**Table S5**). Both DNA and RNA viral communities
601 mirrored beta diversity trends observed in the bacterial and fungal communities; those in mineral
602 soil horizons were less constrained in multivariate space compared to communities in organic
603 horizons, further highlighting the homogenizing influence of wildfire (**Figure S11**). Additionally,
604 DNA and RNA viral community composition was not significantly different between low- and
605 high-severity impacted soils (ANOSIM R = 0.007 and -0.12, respectively; $p > 0.1$) but significantly
606 differed between the two soil horizons (ANOSIM R = 0.59 and 0.57, respectively; $p < 0.05$).

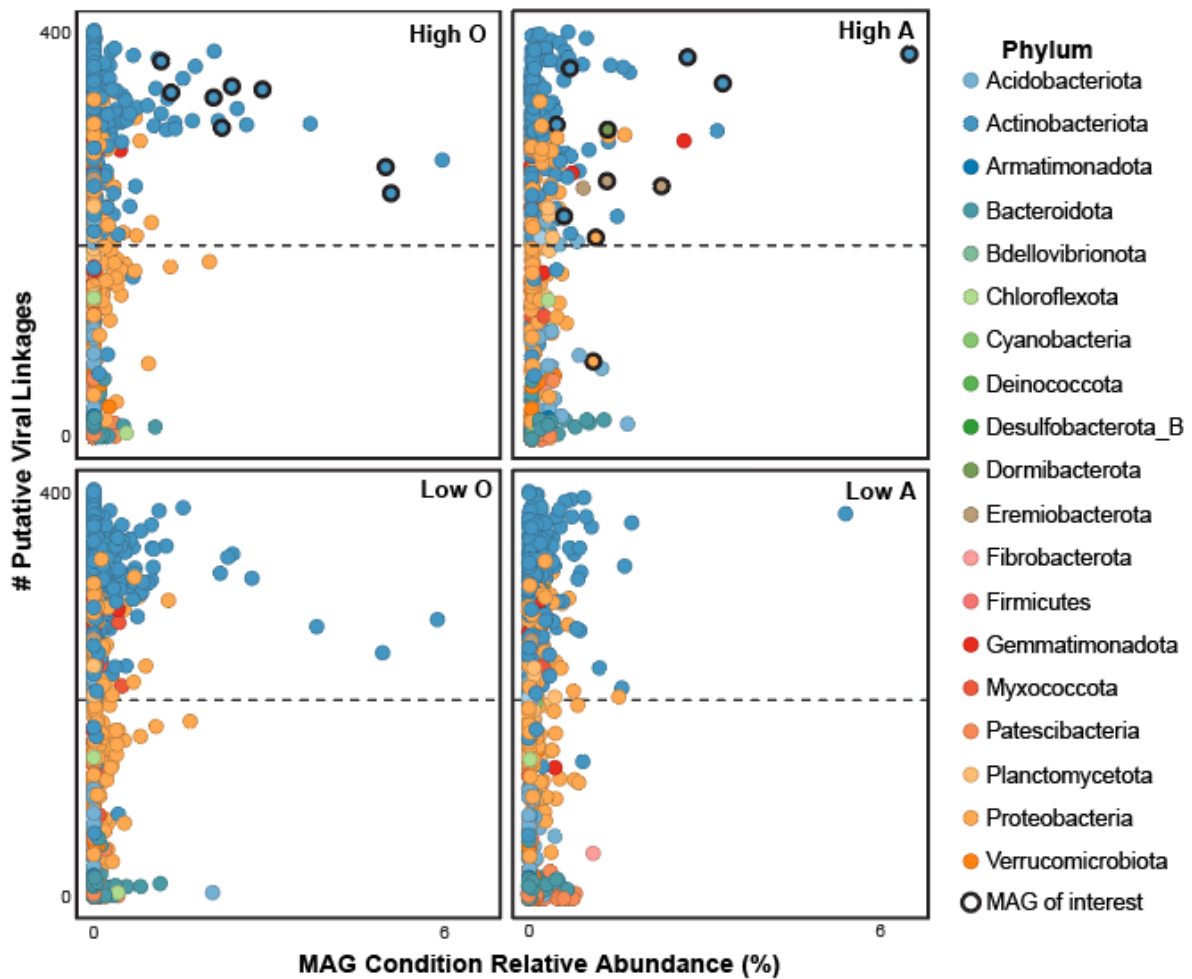
607

608 Given the importance of viral activity on soil microbiome community composition and
609 function^{91,92}, we identified potential virus-host linkages that could offer insights into how viruses
610 target bacteria. Many abundant and active MAGs (n=94) – including 32 from the Actinobacteria
611 – encoded CRISPR-Cas arrays with an average of ~18 spacers (max 210 spacers; **Supplementary**
612 **data 3**). Through the matching of protospacers to sequences in vMAGs, we linked 9 vMAGs with
613 4 bacterial hosts (RYN_115, RYN_242, RYN_436, RYN_542) from the phyla Actinobacteria,
614 Planctomycetota, and Proteobacteria. While each of these four MAGs were active (via transcript
615 expression), the RYN_242 MAG (*Solirubrobacteraceae*) was among the top 3% of active MAGs
616 across all four conditions, suggesting that viruses are targeting active bacteria. We expanded upon
617 potential virus-host linkages using VirHostMatcher⁶⁴ (d_2^* value < 0.25), revealing higher numbers
618 of viral linkages with more abundant host MAGs (**Figure 6**). For example, the MAGs of interest
619 from High O and High A samples had above average numbers of putative viral linkages (average
620 of 196; **Figure 6**). Moreover, there were 198 vMAGs with putative linkages to all 8 featured
621 Actinobacteria MAGs from High O soils, potentially due to conserved nucleotide frequencies. The
622 shared 198 vMAGs made up ~11% of the viral community in High O samples, again suggesting
623 that the most abundant and active bacteria in burned soils are being actively targeted by abundant
624 phage, potentially impacting soil C cycling via release of labile cellular components following cell
625 lysis. There is also evidence in this system for the “piggyback-the-winner” viral strategy, where
626 lysogenic lifestyles are favored at high microbial abundances and growth rates⁹³. Of our 2399
627 DNA vMAGs, we identified 185 with putative lysogenic lifestyles based on gene annotations for
628 integrase, recombinase, or excisionase genes, 32 of which had nucleotide frequency-based
629 linkages to all the featured Actinobacteria MAGs in High O samples.

630

631 To further investigate potential viral roles in C cycling in burned soils, we characterized the
632 putative AMG repertoire of the vMAGs. Viruses utilize AMGs to “hijack” and manipulate the
633 metabolisms of their host; one study in thawing permafrost soils found AMGs associated with
634 SOM degradation and central C metabolism, suggesting that viruses can play a direct role in

635 augmenting the soil C cycle⁹². There were 773 total putative AMGs detected in 445 vMAGs within
636 the FiRE database, including 138 CAZymes targeting diverse substrates such as cellulose, chitin,
637 pectin, and xylan (**Supplementary data 6**). Additionally, the AMGs included 105 genes related
638 to growth (e.g., ribosomal proteins, ribonucleoside-diphosphate reductase), 21 central carbon
639 metabolism genes, and 21 genes encoding peptidases. Over 100 of these genes – including some
640 related to SOM and necromass processing (e.g., glycoside hydrolases, polysaccharide lyases) and
641 cell growth (pyrimidine ribonucleotide biosynthesis) – could be linked to all 8 of the featured High
642 O Actinobacteria MAGs. Furthermore, transcripts mapped to 14 of this subset of AMGs,
643 suggesting that prophage are manipulating SOM degradation metabolisms and potential cell
644 growth rates of active bacterial MAGs in High O samples.



645 **Figure 6.** Each MAG's relative abundance within each respective condition plotted against the
646 number of putative viral linkages identified by VirHostMatcher. Dashed line indicates the
647 database average of 196. Points outlined in bold represent MAGs discussed as important in either
648 High O or High A samples.

649
650
651

652 *Fungal genomes are active across burn conditions*

653 Two fungal Ascomycota MAGs from taxa previously shown to be pyrophilous, *Leotiomyces*
654 (R113-184) and *Coniochaeta ligniaria* (R110-5)^{68,94–96}, were reconstructed from the
655 metagenomic data. These taxa were prominently represented in our ITS amplicon data; the
656 *Leotiomyces* class increased in relative abundance by ~215% between control and High O
657 samples (14% to 45%) and the *Coniochaeta* genus relative abundance increased from 0.003% to
658 1% from control to High A soils.

659
660 Complementing observations from pyrophilous bacterial MAGs, the fungal MAGs encoded and
661 expressed genes for degrading aromatic compounds, including both the upper (peripheral)
662 pathways for diverse aromatic substrates and lower pathways targeting intermediates catechol or
663 protocatechuate. Each MAG expressed genes for degrading salicylate (salicylate hydroxylase),
664 phenol (phenol 2-monooxygenase), and catechol (catechol 1,2-dioxygenase), and expression of all
665 three genes increased from low to high severity in both soil horizons. The MAGs also encoded
666 laccases, which are enriched in pyrophilous fungal genomes⁹⁷ and act on aromatic substrates⁹⁸.
667 The *Coniochaeta* MAG additionally encoded hydrophobic surface binding proteins (*hsbA*;
668 PF12296) which may facilitate the degradation of fire-derived hydrophobic compounds and be
669 critical to soil recovery⁹⁷. To directly compare the fungal and bacterial contribution to catechol
670 degradation, we compared the number of normalized transcriptomic reads recruited to the gene
671 encoding catechol 1,2-dioxygenase, *catA*. In High O samples, the fungal MAGs generated more
672 than twice the number of transcripts per gene compared to bacterial MAGs, indicating the
673 significant role that fungi likely play in aromatic DOM degradation in burned soils. Both fungal
674 MAGs can also potentially degrade necromass from lysed heat-sensitive taxa through the
675 expression of diverse peptidases (**Figure S12**), with increased expression from low to high fire
676 severity in both organic and mineral horizons (~40.4% and 235%, respectively).

677
678 *Ecosystem implications*

679 We observed short-term changes in microbiome composition and function that likely alter
680 biogeochemical cycling and initial post-fire vegetation recovery. Both bacterial and fungal
681 community diversity decreased with burn severity (**Figure 2E, F**); a decrease in soil microbiome
682 diversity can influence ecosystem function⁹⁹. Despite the key role that bacterial N-fixing bacteria
683 and mycorrhizal fungi play in generating plant available N pools¹⁴ (up to 80% of N acquired by
684 plants in boreal and temperate forests), we found no expression of the functional gene catalyzing
685 N fixation (*nifH*). Further, despite the three-fold increase in soil mineral soil ammonium observed
686 in this study (**Supplementary data 1**) and others¹⁰⁰, the gene that catalyzes ammonia oxidation
687 (*amoA*) was absent from the MAG database. These observations mirror trends reported by other
688 studies; short-term, post-fire decreases in the abundances of N-fixation and ammonia-oxidation
689 genes have been noted in a mixed conifer forest¹⁰¹. Further highlighting potential reductions in
690 metabolic function within the post-fire community, we also note that MAGs active in High O

691 samples express fewer CAZymes that target a less diverse array of C substrates relative to High A
692 MAGs (**Figure S6**), suggesting that certain C cycling processes may be absent in High O samples.
693

694 Ectomycorrhizal fungi (EMF) facilitate plant access to limiting nutrients and water in return for
695 carbohydrates derived from photosynthesis¹⁰². We observed a 99% decrease in EMF relative
696 abundance across the burn severity gradient (**Table S3**) from direct heat-induced or subsequent
697 death of their plant hosts¹⁸, which likely has implications for obligate host plants such as *P.*
698 *contorta*, the dominant tree species in these forests. For example, we found that *Cenocccum*
699 *geophilum*, a common EMF symbiont of *P. contorta*^{103,104} was present in our unburned sites but
700 absent after burning. Although we observed loss of EMF the year after severe wildfire, research in
701 nearby forests indicates high (>90%) EMF colonization of pine roots within a decade of burning¹⁰⁵.

702
703 Lastly, we show that wildfire and the post-fire soil chemical environment results in a microbiome
704 that actively degrades aromatic compounds likely formed during fire (**Figure 5**). This finding
705 supports recent studies suggesting that pyrogenic organic carbon is more labile than previously
706 thought¹⁰⁶, with implications for the modeling of C storage in wildfire impacted ecosystems.
707 Further work is needed integrating multi-omics data from both field observations and laboratory
708 experiments into ecosystem models to refine the quantification of C fluxes in post-fire ecosystems.

709

710 **Conclusion**

711 Here we present FiRE-db, a publicly available, comprehensive genome database of pyrophilous
712 microorganisms that provides functional context to observed shifts in soil microbiome structure
713 following wildfire. Our results indicate that dominant microorganisms occupy available post-fire
714 niche space through a combination of strategies, including heat tolerance, fast growth, and the
715 utilization of substrates available post-fire. This ability to use aromatic DOM that is likely
716 generated during wildfire is widespread throughout the bacterial and fungal community, with
717 implications for assumptions regarding the residence time of pyrogenic carbon. Carbon processing
718 within the system is also influenced by the presence and activity of abundant viruses that target
719 key bacterial community members through viral predation and activity of AMGs. The measured
720 patterns of community dynamics are both consistent across fires and trophic levels (i.e., bacteria,
721 fungi, and viruses), offering opportunities to leverage these results for more effective management
722 of other wildfire-disturbed environments.

723

724 **Acknowledgements**

725 This work was supported through a USDA NIFA award (#2021-67019-34608) to MJW. FTICR
726 MS analyses were performed under the Facilities Integrating Collaborations for User Science
727 (FICUS) initiative and used resources at the Environmental Molecular Sciences Laboratory
728 (proposal ID 49615), which is a DOE Office of Science User Facilities. This facility is sponsored
729 by the Office of Biological and Environmental Research and operated under contract number DE-
730 AC05-76RL01830. Metagenomic and metatranscriptomic sequencing was performed at the

731 University of Colorado Cancer Center's Genomics Shared Resource, which is supported by the
732 Cancer Center Support Grant P30CA046934. This work utilized resources from the University of
733 Colorado Boulder Research Computing Group, which is supported by the National Science
734 Foundation (awards ACI-1532235 and ACI-1532236), the University of Colorado Boulder, and
735 Colorado State University. The work conducted by the U.S. Department of Energy Joint Genome
736 Institute, a DOE Office of Science User Facility, is supported by the Office of Science of the U.S.
737 Department of Energy under Contract No. DE-AC02-05CH11231. We thank Fabiola Pulido-
738 Chavez for help with processing the ITS amplicon sequencing data.

739

740 **Author contributions**

741 ARN, CCR, and MJW designed the field sampling and downstream analyses. ARN, KKA, and
742 MJW performed field sampling, while ARN and RAD performed laboratory sample processing.
743 ARN and ABN led the microbial analyses, with assistance from SM, ASS, IG, and AS for fungal
744 genomics. JBE and SEG assisted with viral interpretations, while HR, TB, RC, and RY contributed
745 with high-resolution carbon measurements and analyses. TF performed bulk soil geochemistry
746 measurements. ARN, CCR, and MJW wrote the manuscript, with assistance and input from all co-
747 authors.

748

749 **Competing interest statement**

750 The authors declare no competing interests.

751

752 **References**

- 753 1. Dennison, P. E., Brewer, S. C., Arnold, J. D. & Moritz, M. A. Large wildfire trends in the
754 western United States, 1984-2011. *Geophys. Res. Lett.* **41**, 2928–2933 (2014).
- 755 2. Higuera, P. E. & Abatzoglou, J. T. Record-setting climate enabled the extraordinary 2020
756 fire season in the western United States. *Glob. Chang. Biol.* gcb.15388 (2020).
757 doi:10.1111/gcb.15388
- 758 3. Parks, S. A. & Abatzoglou, J. T. Warmer and Drier Fire Seasons Contribute to Increases
759 in Area Burned at High Severity in Western US Forests From 1985 to 2017. *Geophys.*
760 *Res. Lett.* **47**, 1–10 (2020).
- 761 4. Tran, B. N., Tanase, M. A., Bennett, L. T. & Aponte, C. High-severity wildfires in
762 temperate Australian forests have increased in extent and aggregation in recent decades.
763 *PLoS One* **15**, e0242484 (2020).
- 764 5. Benavides-Solorio, J. D. D. & MacDonald, L. H. Measurement and prediction of post-fire
765 erosion at the hillslope scale, Colorado Front Range. *Int. J. Wildl. Fire* **14**, 457 (2005).
- 766 6. Pierson, D. N., Robichaud, P. R., Rhoades, C. C. & Brown, R. E. Soil carbon and nitrogen
767 eroded after severe wildfire and erosion mitigation treatments. *Int. J. Wildl. Fire* **28**, 814
768 (2019).
- 769 7. Rhoades, C. C., Entwistles, D. & Butler, D. The influence of wildfire extent and severity
770 on streamwater chemistry, sediment and temperature following the Hayman Fire ,
771 Colorado. *Int. J. Wildl. Fire* 430–442 (2011).
- 772 8. Riggan, P. J. *et al.* Effects of fire severity on nitrate mobilization in watersheds subject to
773 chronic atmospheric deposition. *Environ. Sci. Technol.* **28**, 369–375 (1994).

- 774 9. Chambers, M. E., Fornwalt, P. J., Malone, S. L. & Battaglia, M. A. Patterns of conifer
775 regeneration following high severity wildfire in ponderosa pine – dominated forests of the
776 Colorado Front Range. *For. Ecol. Manage.* **378**, 57–67 (2016).
- 777 10. Harvey, B. J., Donato, D. C. & Turner, M. G. High and dry: Post-fire tree seedling
778 establishment in subalpine forests decreases with post-fire drought and large stand-
779 replacing burn patches. *Glob. Ecol. Biogeogr.* **25**, 655–669 (2016).
- 780 11. Rammer, W. *et al.* Widespread regeneration failure in forests of Greater Yellowstone
781 under scenarios of future climate and fire. *Glob. Chang. Biol.* gcb.15726 (2021).
782 doi:10.1111/gcb.15726
- 783 12. Rhoades, C. C. *et al.* The Legacy of a Severe Wildfire on Stream Nitrogen and Carbon in
784 Headwater Catchments. *Ecosystems* **22**, 643–657 (2019).
- 785 13. Strickland, M. S., Lauber, C., Fierer, N. & Bradford, M. A. Testing the functional
786 significance of microbial community composition. *Ecology* **90**, 441–451 (2009).
- 787 14. van der Heijden, M. G. A., Bardgett, R. D. & van Straalen, N. M. The unseen majority:
788 soil microbes as drivers of plant diversity and productivity in terrestrial ecosystems. *Ecol.*
789 *Lett.* **11**, 296–310 (2008).
- 790 15. Mendes, R. *et al.* Deciphering the Rhizosphere Microbiome for Disease-Suppressive
791 Bacteria. *Science (80-.)*. **332**, 1097–1100 (2011).
- 792 16. Pressler, Y., Moore, J. C. & Cotrufo, M. F. Belowground community responses to fire:
793 meta-analysis reveals contrasting responses of soil microorganisms and mesofauna. *Oikos*
794 **128**, 309–327 (2019).
- 795 17. Fernández-González, A. J. *et al.* The rhizosphere microbiome of burned holm-oak:
796 potential role of the genus *Arthrobacter* in the recovery of burned soils. *Sci. Rep.* **7**, 6008
797 (2017).
- 798 18. Pulido-Chavez, M. F., Alvarado, E. C., DeLuca, T. H., Edmonds, R. L. & Glassman, S. I.
799 High-severity wildfire reduces richness and alters composition of ectomycorrhizal fungi in
800 low-severity adapted ponderosa pine forests. *For. Ecol. Manage.* **485**, 118923 (2021).
- 801 19. Sáenz de Miera, L. E., Pinto, R., Gutierrez-Gonzalez, J. J., Calvo, L. & Ansola, G.
802 Wildfire effects on diversity and composition in soil bacterial communities. *Sci. Total*
803 *Environ.* **726**, 138636 (2020).
- 804 20. Villadas, P. J. *et al.* The Soil Microbiome of the Laurel Forest in Garajonay National Park
805 (La Gomera, Canary Islands): Comparing Unburned and Burned Habitats after a Wildfire.
806 *Forests* **10**, 1051 (2019).
- 807 21. van der Voort, M., Kempenaar, M., van Driel, M., Raaijmakers, J. M. & Mendes, R.
808 Impact of soil heat on reassembly of bacterial communities in the rhizosphere microbiome
809 and plant disease suppression. *Ecol. Lett.* **19**, 375–382 (2016).
- 810 22. Ibáñez, T. S., Wardle, D. A., Gundale, M. J. & Nilsson, M.-C. Effects of Soil Abiotic and
811 Biotic Factors on Tree Seedling Regeneration Following a Boreal Forest Wildfire.
812 *Ecosystems* (2021). doi:10.1007/s10021-021-00666-0
- 813 23. Lucas-Borja, M. E. *et al.* Immediate fire-induced changes in soil microbial community
814 composition in an outdoor experimental controlled system. *Sci. Total Environ.* **696**,
815 (2019).
- 816 24. Cobo-Díaz, J. F. *et al.* Metagenomic Assessment of the Potential Microbial Nitrogen
817 Pathways in the Rhizosphere of a Mediterranean Forest After a Wildfire. *Microb. Ecol.*
818 **69**, 895–904 (2015).
- 819 25. Tas, N. *et al.* Impact of fire on active layer and permafrost microbial communities and

- 820 metagenomes in an upland Alaskan boreal forest. *ISME J.* 1904–1919 (2014).
821 doi:10.1038/ismej.2014.36
- 822 26. Parson, A., Robichaud, P. R., Lewis, S. A., Napper, C. & Clark, J. T. *Field guide for*
823 *mapping post-fire soil burn severity. USDA Forest Service - General Technical Report*
824 *RMRS-GTR* (2010). doi:10.2737/RMRS-GTR-243
- 825 27. Miesel, J. R., Hockaday, W. C., Kolka, R. K. & Townsend, P. A. Soil organic matter
826 composition and quality across fire severity gradients in coniferous and deciduous forests
827 of the southern boreal region. *J. Geophys. Res. Biogeosciences* **120**, 1124–1141 (2015).
- 828 28. Bundy, L. G. & Meisinger, J. J. Nitrogen Availability Indices. in *Methods of Soil*
829 *Analysis: Part 2 Microbiological and Biochemical Properties* 951–984 (Macmillan
830 Education UK, 2018). doi:10.2136/sssabookser5.2.c41
- 831 29. Dittmar, T., Koch, B., Hertkorn, N. & Kattner, G. A simple and efficient method for the
832 solid-phase extraction of dissolved organic matter (SPE-DOM) from seawater. *Limnol.*
833 *Oceanogr. Methods* **6**, 230–235 (2008).
- 834 30. Tolić, N. *et al.* Formularity: Software for Automated Formula Assignment of Natural and
835 Other Organic Matter from Ultrahigh-Resolution Mass Spectra. *Anal. Chem.* **89**, 12659–
836 12665 (2017).
- 837 31. Bramer, L. M. *et al.* ftmsRanalysis: An R package for exploratory data analysis and
838 interactive visualization of FT-MS data. *PLOS Comput. Biol.* **16**, e1007654 (2020).
- 839 32. Bramer, L. M. & White, A. ftmsRanalysis: Analysis and visualization tools for FT-MS
840 data. R package version 1.0.0. (2019).
- 841 33. Caporaso, J. G. *et al.* Ultra-high-throughput microbial community analysis on the Illumina
842 HiSeq and MiSeq platforms. *ISME J.* **6**, 1621–1624 (2012).
- 843 34. Quast, C. *et al.* The SILVA ribosomal RNA gene database project: improved data
844 processing and web-based tools. *Nucleic Acids Res.* **41**, D590–D596 (2012).
- 845 35. Kõljalg, U. *et al.* UNITE: a database providing web-based methods for the molecular
846 identification of ectomycorrhizal fungi. *New Phytol.* **166**, 1063–1068 (2005).
- 847 36. Bolyen, E. *et al.* Reproducible, interactive, scalable and extensible microbiome data
848 science using QIIME 2. *Nat. Biotechnol.* **37**, 852–857 (2019).
- 849 37. Nguyen, N. H. *et al.* FUNGuild: An open annotation tool for parsing fungal community
850 datasets by ecological guild. *Fungal Ecol.* **20**, 241–248 (2016).
- 851 38. Team, R. C. R: A language and environment for statistical computing. *R Found. Stat.*
852 *Comput. Vienna, Austria* (2021).
- 853 39. Oksanen, J. *et al.* Package ‘vegan’. in (Springer Netherlands, 2013). doi:10.1007/978-94-
854 024-1179-9_301576
- 855 40. McMurdie, P. J. & Holmes, S. phyloseq: An R Package for Reproducible Interactive
856 Analysis and Graphics of Microbiome Census Data. *PLoS One* **8**, e61217 (2013).
- 857 41. Segata, N. *et al.* Metagenomic biomarker discovery and explanation. *Genome Biol.* **12**,
858 R60 (2011).
- 859 42. Joshi, N. & Fass, J. Sickle: A sliding-window, adaptive, quality-based trimming tool for
860 FastQ files. (2011).
- 861 43. Li, D., Liu, C.-M., Luo, R., Sadakane, K. & Lam, T.-W. MEGAHIT: an ultra-fast single-
862 node solution for large and complex metagenomics assembly via succinct de Bruijn graph.
863 *Bioinformatics* **31**, 1674–1676 (2015).
- 864 44. Kang, D. D. *et al.* MetaBAT 2: an adaptive binning algorithm for robust and efficient
865 genome reconstruction from metagenome assemblies. *PeerJ* **7**, e7359 (2019).

- 866 45. Parks, D. H., Imelfort, M., Skennerton, C. T., Hugenholtz, P. & Tyson, G. W. CheckM:
867 assessing the quality of microbial genomes recovered from isolates, single cells, and
868 metagenomes. *Genome Res.* **25**, 1043–1055 (2015).
- 869 46. Chaumeil, P.-A., Mussig, A. J., Hugenholtz, P. & Parks, D. H. GTDB-Tk: a toolkit to
870 classify genomes with the Genome Taxonomy Database. *Bioinformatics* **36**, 1925–1927
871 (2019).
- 872 47. Olm, M. R., Brown, C. T., Brooks, B. & Banfield, J. F. dRep: a tool for fast and accurate
873 genomic comparisons that enables improved genome recovery from metagenomes through
874 de-replication. *ISME J.* **11**, 2864–2868 (2017).
- 875 48. Bowers, R. M. *et al.* Minimum information about a single amplified genome (MISAG)
876 and a metagenome-assembled genome (MIMAG) of bacteria and archaea. *Nat.*
877 *Biotechnol.* **35**, 725–731 (2017).
- 878 49. Weissman, J. L., Hou, S. & Fuhrman, J. A. Estimating maximal microbial growth rates
879 from cultures, metagenomes, and single cells via codon usage patterns. *PNAS* **118**, 1–10
880 (2020).
- 881 50. Bushmanova, E., Antipov, D., Lapidus, A. & Prjibelski, A. D. RnaSPAdes: A de novo
882 transcriptome assembler and its application to RNA-Seq data. *Gigascience* **8**, 1–13 (2019).
- 883 51. Grigoriev, I. V. *et al.* MycoCosm portal: Gearing up for 1000 fungal genomes. *Nucleic*
884 *Acids Res.* **42**, 699–704 (2014).
- 885 52. Shaffer, M. *et al.* DRAM for distilling microbial metabolism to automate the curation of
886 microbiome function. *Nucleic Acids Res.* **48**, 8883–8900 (2020).
- 887 53. Eddy, S. R. Accelerated profile HMM searches. *PLoS Comput. Biol.* **7**, (2011).
- 888 54. Aramaki, T. *et al.* KofamKOALA: KEGG Ortholog assignment based on profile HMM
889 and adaptive score threshold. *Bioinformatics* **36**, 2251–2252 (2020).
- 890 55. Anders, S., Pyl, P. T. & Huber, W. HTSeq—a Python framework to work with high-
891 throughput sequencing data. *Bioinformatics* **31**, 166–169 (2015).
- 892 56. Love, M. I., Huber, W. & Anders, S. Moderated estimation of fold change and dispersion
893 for RNA-seq data with DESeq2. *Genome Biol.* **15**, 550 (2014).
- 894 57. Smid, M. *et al.* Gene length corrected trimmed mean of M-values (GeTMM) processing of
895 RNA-seq data performs similarly in intersample analyses while improving intrasample
896 comparisons. *BMC Bioinformatics* **19**, 236 (2018).
- 897 58. Robinson, M. D., McCarthy, D. J. & Smyth, G. K. edgeR: a Bioconductor package for
898 differential expression analysis of digital gene expression data. *Bioinformatics* **26**, 139–
899 140 (2010).
- 900 59. Guo, J. *et al.* VirSorter2: a multi-classifier, expert-guided approach to detect diverse DNA
901 and RNA viruses. *Microbiome* **9**, 37 (2021).
- 902 60. Nayfach, S. *et al.* CheckV assesses the quality and completeness of metagenome-
903 assembled viral genomes. *Nat. Biotechnol.* **39**, 578–585 (2021).
- 904 61. Guo, J., Vik, D., Pratama, A. A., Roux, S. & Sullivan, M. B. Viral sequence identification
905 SOP with VirSorter2. (2021). doi:10.17504/protocols.io.btv8nn9w
- 906 62. Bland, C. *et al.* CRISPR recognition tool (CRT): a tool for automatic detection of
907 clustered regularly interspaced palindromic repeats. *BMC Bioinformatics* **8**, 209 (2007).
- 908 63. Skennerton, C. T., Imelfort, M. & Tyson, G. W. Crass: identification and reconstruction of
909 CRISPR from unassembled metagenomic data. *Nucleic Acids Res.* **41**, e105–e105 (2013).
- 910 64. Ahlgren, N. A., Ren, J., Lu, Y. Y., Fuhrman, J. A. & Sun, F. Alignment-free $\$d_2^*$
911 oligonucleotide frequency dissimilarity measure improves prediction of hosts from

- 912 metagenomically-derived viral sequences. *Nucleic Acids Res.* **45**, 39–53 (2017).
- 913 65. Weber, C. F., Lockhart, J. S., Charaska, E., Aho, K. & Lohse, K. A. Bacterial composition
914 of soils in ponderosa pine and mixed conifer forests exposed to different wildfire burn
915 severity. *Soil Biol. Biochem.* **69**, 242–250 (2014).
- 916 66. Whitman, T. *et al.* Soil bacterial and fungal response to wildfires in the Canadian boreal
917 forest across a burn severity gradient. *Soil Biol. Biochem.* **138**, 107571 (2019).
- 918 67. Reazin, C., Morris, S., Smith, J. E., Cowan, A. D. & Jumpponen, A. Fires of differing
919 intensities rapidly select distinct soil fungal communities in a Northwest US ponderosa
920 pine forest ecosystem. *For. Ecol. Manage.* **377**, 118–127 (2016).
- 921 68. Yang, T. *et al.* Distinct fungal successional trajectories following wildfire between soil
922 horizons in a cold-temperate forest. *New Phytol.* **227**, 572–587 (2020).
- 923 69. Adkins, J., Docherty, K. M., Gutknecht, J. L. M. & Miesel, J. R. How do soil microbial
924 communities respond to fire in the intermediate term? Investigating direct and indirect
925 effects associated with fire occurrence and burn severity. *Sci. Total Environ.* **745**, 140957
926 (2020).
- 927 70. Lucas-Borja, M. E. *et al.* Immediate fire-induced changes in soil microbial community
928 composition in an outdoor experimental controlled system. *Sci. Total Environ.* **696**,
929 134033 (2019).
- 930 71. Woollet, J. *et al.* Short-interval reburns in the boreal forest alter soil bacterial communities,
931 reflecting increased pH and poor conifer seedling establishment. *bioRxiv* (2021).
932 doi:10.1101/2021.03.31.437944
- 933 72. Newton, G. L., Buchmeier, N. & Fahey, R. C. Biosynthesis and Functions of Mycothiol,
934 the Unique Protective Thiol of Actinobacteria. *Microbiol. Mol. Biol. Rev.* **72**, 471–494
935 (2008).
- 936 73. Richter, A. A. *et al.* Biosynthesis of the Stress-Protectant and Chemical Chaperon Ectoine:
937 Biochemistry of the Transaminase EctB. *Front. Microbiol.* **10**, 1–20 (2019).
- 938 74. Musto, H. *et al.* Correlations between genomic GC levels and optimal growth
939 temperatures in prokaryotes. *FEBS Lett.* **573**, 73–77 (2004).
- 940 75. Yakovchuk, P. Base-stacking and base-pairing contributions into thermal stability of the
941 DNA double helix. *Nucleic Acids Res.* **34**, 564–574 (2006).
- 942 76. Mooshammer, M. *et al.* Decoupling of microbial carbon, nitrogen, and phosphorus cycling
943 in response to extreme temperature events. *Sci. Adv.* **3**, e1602781 (2017).
- 944 77. Donhauser, J., Qi, W., Bergk-Pinto, B. & Frey, B. High temperatures enhance the
945 microbial genetic potential to recycle C and N from necromass in high-mountain soils.
946 *Glob. Chang. Biol.* 1–22 (2020). doi:10.1111/gcb.15492
- 947 78. Pérez-Valera, E., Goberna, M. & Verdú, M. Fire modulates ecosystem functioning
948 through the phylogenetic structure of soil bacterial communities. *Soil Biol. Biochem.* **129**,
949 80–89 (2019).
- 950 79. Long, A. M., Hou, S., Ignacio-Espinoza, J. C. & Fuhrman, J. A. Benchmarking microbial
951 growth rate predictions from metagenomes. *ISME J.* **15**, 183–195 (2021).
- 952 80. Vieira-Silva, S. & Rocha, E. P. C. The Systemic Imprint of Growth and Its Uses in
953 Ecological (Meta)Genomics. *PLoS Genet.* **6**, e1000808 (2010).
- 954 81. McCormick, J. R. & Flärdh, K. Signals and regulators that govern *Streptomyces*
955 development. *FEMS Microbiol. Rev.* **36**, 206–231 (2012).
- 956 82. Chater, K. F., Biró, S., Lee, K. J., Palmer, T. & Schrepf, H. The complex extracellular
957 biology of *Streptomyces*. *FEMS Microbiol. Rev.* **34**, 171–198 (2010).

- 958 83. Lu, X., Heal, K. R., Ingalls, A. E., Doxey, A. C. & Neufeld, J. D. Metagenomic and
959 chemical characterization of soil cobalamin production. *ISME J.* **14**, 53–66 (2020).
- 960 84. Doxey, A. C., Kurtz, D. A., Lynch, M. D. J., Sauder, L. A. & Neufeld, J. D. Aquatic
961 metagenomes implicate Thaumarchaeota in global cobalamin production. *ISME J.* **9**, 461–
962 471 (2015).
- 963 85. Palacios, O. A., Bashan, Y. & De-Bashan, L. E. Proven and potential involvement of
964 vitamins in interactions of plants with plant growth-promoting bacteria—an overview.
965 *Biol. Fertil. Soils* **50**, 415–432 (2014).
- 966 86. Akduman, N. *et al.* Bacterial vitamin B12 production enhances nematode predatory
967 behavior. *ISME J.* **14**, 1494–1507 (2020).
- 968 87. Faria, S. R. *et al.* Wildfire-induced alterations of topsoil organic matter and their recovery
969 in Mediterranean eucalypt stands detected with biogeochemical markers. *Eur. J. Soil Sci.*
970 **66**, 699–713 (2015).
- 971 88. Fernández, I., Cabaneiro, A. & Carballas, T. Organic matter changes immediately after a
972 wildfire in an atlantic forest soil and comparison with laboratory soil heating. *Soil Biol.*
973 *Biochem.* **29**, 1–11 (1997).
- 974 89. LaRowe, D. E. & Van Cappellen, P. Degradation of natural organic matter: A
975 thermodynamic analysis. *Geochim. Cosmochim. Acta* **75**, 2030–2042 (2011).
- 976 90. Fuchs, G., Boll, M. & Heider, J. Microbial degradation of aromatic compounds- From one
977 strategy to four. *Nat. Rev. Microbiol.* **9**, 803–816 (2011).
- 978 91. Emerson, J. B. *et al.* Host-linked soil viral ecology along a permafrost thaw gradient. *Nat.*
979 *Microbiol.* **3**, 870–880 (2018).
- 980 92. Trubl, G. *et al.* Soil Viruses Are Underexplored Players in Ecosystem Carbon Processing.
981 *mSystems* **3**, 1–21 (2018).
- 982 93. Knowles, B. *et al.* Lytic to temperate switching of viral communities. *Nature* **531**, 466–
983 470 (2016).
- 984 94. Ammitzboll, H., Jordan, G. J., Baker, S. C., Freeman, J. & Bissett, A. Diversity and
985 abundance of soil microbial communities decline, and community compositions change
986 with severity of post-logging fire. *Mol. Ecol.* **mec.15900** (2021). doi:10.1111/mec.15900
- 987 95. Hewelke, E. *et al.* Soil Functional Responses to Natural Ecosystem Restoration of a Pine
988 Forest Peucedano-Pinetum after a Fire. *Forests* **11**, 286 (2020).
- 989 96. Mahoney, D. P. & LaFavre, J. S. *Coniochaeta extramundana*, with a Synopsis of Other
990 *Coniochaeta* Species. *Mycologia* **73**, 931 (1981).
- 991 97. Steindorff, A. S. *et al.* Comparative genomics of pyrophilous fungi reveals a link between
992 fire events and developmental genes. *Environ. Microbiol.* **23**, 99–109 (2021).
- 993 98. Viswanath, B., Rajesh, B., Janardhan, A., Kumar, A. P. & Narasimha, G. Fungal Laccases
994 and Their Applications in Bioremediation. *Enzyme Res.* **2014**, 1–21 (2014).
- 995 99. Wagg, C., Schlaeppi, K., Banerjee, S., Kuramae, E. E. & van der Heijden, M. G. A.
996 Fungal-bacterial diversity and microbiome complexity predict ecosystem functioning. *Nat.*
997 *Commun.* **10**, 4841 (2019).
- 998 100. Wan, S., Hui, D. & Luo, Y. Fire effects on nitrogen pools and dynamics in terrestrial
999 ecosystems: A meta-analysis. *Ecol. Appl.* **11**, 1349–1365 (2001).
- 1000 101. Yeager, C. M., Northup, D. E., Grow, C. C., Barns, S. M. & Kuske, C. R. Changes in
1001 nitrogen-fixing and ammonia-oxidizing bacterial communities in soil of a mixed conifer
1002 forest after wildfire. *Appl. Environ. Microbiol.* **71**, 2713–2722 (2005).
- 1003 102. Smith, S. E. & Read, D. Mycorrhizal Symbiosis. *Soil Sci.* **137**, 204 (1984).

- 1004 103. Garcia, M. O., Smith, J. E., Luoma, D. L. & Jones, M. D. Ectomycorrhizal communities
1005 of ponderosa pine and lodgepole pine in the south-central Oregon pumice zone.
1006 *Mycorrhiza* **26**, 275–286 (2016).
- 1007 104. Douglas, R. B., Parker, V. T. & Cullings, K. W. Belowground ectomycorrhizal
1008 community structure of mature lodgepole pine and mixed conifer stands in Yellowstone
1009 National Park. *For. Ecol. Manage.* **208**, 303–317 (2005).
- 1010 105. Rhoades, C. C., Fegel, T. S., Zaman, T., Fornwalt, P. J. & Miller, S. P. Are soil changes
1011 responsible for persistent slash pile burn scars in lodgepole pine forests? *For. Ecol.*
1012 *Manage.* **490**, (2021).
- 1013 106. Graham, E. B. *et al.* Inferred bioavailability of pyrogenic organic matter compared to
1014 natural organic matter from global sediments and surface waters. *EcoEvoRxiv* (2021).
1015 doi:10.32942/osf.io/6j9t5
1016
1017
1018
1019
1020
1021